ACS OMEGA

http://pubs.acs.org/journal/acsodf

Article

Silica Magnetic Graphene Oxide Improves the Effects of Stem Cell-Conditioned Medium on Acute Liver Failure

Tahereh Foroutan,* Fahimeh Kabiri, and Elaheh Motamedi

Cite This: *ACS Omega* 2021, 6, 21194−21206

Read Online

ACCESS | Metrics & More | Article Recommendations

ABSTRACT: Objective: Acute liver failure (ALF) is usually associated with inflammation and oxidation of hepatocytes and has high mortality and resource costs. Although mesenchymal stem cell-conditioned medium (MSC-CM) has therapeutic effects similar to MSC transplant in treating liver failure, it may not increase survival. On the other hand, graphene-based nanostructures have been proven useful in biomedicine. In this study, we investigated whether silica magnetic graphene oxide (SMGO) improved the effects of MSC-CM in protecting hepatocytes and stimulating the regeneration of damaged liver cells. Materials and methods: To provide a rat model of ALF, male rats were injected intraperitoneally with carbon tetrachloride (CCl_4). The rats were randomly divided into six groups, namely control, sham, CCl_4, MSC-CM, SMGO, and MSC-CM + SMGO. In the experimental groups, the rats received, depending on the group, 2 mL/kg body weight CCl_4 and either MSC-CM with 5×10^6 MSCs or 300 μg/kg body weight SMGO or both. Symptoms of ALF appeared 4 days after the injection. All groups were compared and analyzed both histologically and biochemically 4 days after the injection. Results: The results indicated that the use of SMGO enhanced the effect of MSC-CM in reducing necrosis, inflammation, aspartate transaminase, alanine aminotransferase, and alkaline phosphatase in the CCl_4-induced liver failure of the rat model. Also, the expression of vascular endothelial growth factor and matrix metalloproteinase-9 (MMP-9) was significantly upregulated after treatment with SMGO. Conclusion: SMGO improved the hepatoprotective effects of MSC-CM on acute liver damage, probably by suppressing necrosis, apoptosis, and inflammation of hepatocytes.

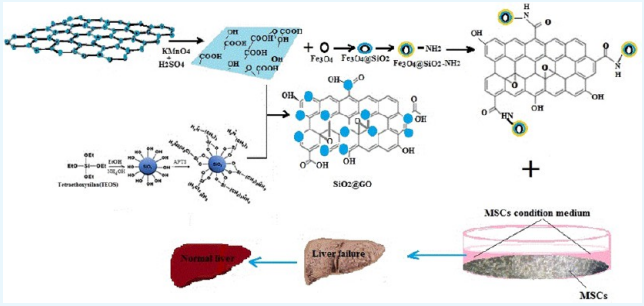

INTRODUCTION

Acute liver failure (ALF) is a life-threatening clinical syndrome characterized by rapid hepatocellular necrosis due to hepatotoxicity, viral infection, and immune-mediated attacks.[1,2] It has high mortality and resource costs.[3] Liver transplantation has some limitations such as the lack of donors, costs, and immunosuppressive complications.[4] Mesenchymal stem cells (MSCs) have also been used to treat ALF. They are easy to obtain and do not pose an ethical problem.[5] MSCs have functions such as secretion of growth factors, angiogenesis, and immunosuppression, as well as properties such as anti-inflammatory and antiapoptosis effects. They can also prevent hepatocyte cell death and stimulate the regeneration of liver cells by the paracrine mechanism or direct differentiation.[2,6]

In view of the ALF treatment with stem cells, the available data are somewhat contradictory. Although MSC injection has some benefits,[7−11] it has occasionally been reported to have no beneficial effect due to poor transplantation and the survival of implanted cells.[12−14] In addition, the failure of MSCs to adhere to the target tissue leads to apoptosis of MSCs.[14] MSC-conditioned medium (MSC-CM) has also recently been shown to have therapeutic effects similar to those of MSC transplants in treating liver failure.[2,15] It has a direct inhibitory effect on hepatocyte apoptosis and promotes hepatocyte proliferation, both in vitro and in vivo. Therefore, MSC-CM transplantation into recipients may be an effective way to reduce liver damage.[6] Embryonic stem cell-derived MSCs (ESC-MSC), on the other hand, induce a higher hepatocyte proliferation rate and have stronger anti-inflammatory properties than bone marrow MSCs. Although MSC-CM and ESC-MSC improve liver function, they do not increase survival.[16]

Today, in addition to different lasers and stem cells, the use of nanomaterials has attracted a great deal of attention in regenerative medicine.[17−22] For instance, graphene and its derivatives have been shown to improve the proliferation and differentiation of stem cells.[23] Due to their physicochemical properties and biocompatibility, which are comparable to

Received: November 4, 2020
Accepted: July 28, 2021
Published: August 10, 2021

https://doi.org/10.1021/acsomega.0c05395
ACS Omega 2021, 6, 21194−21206

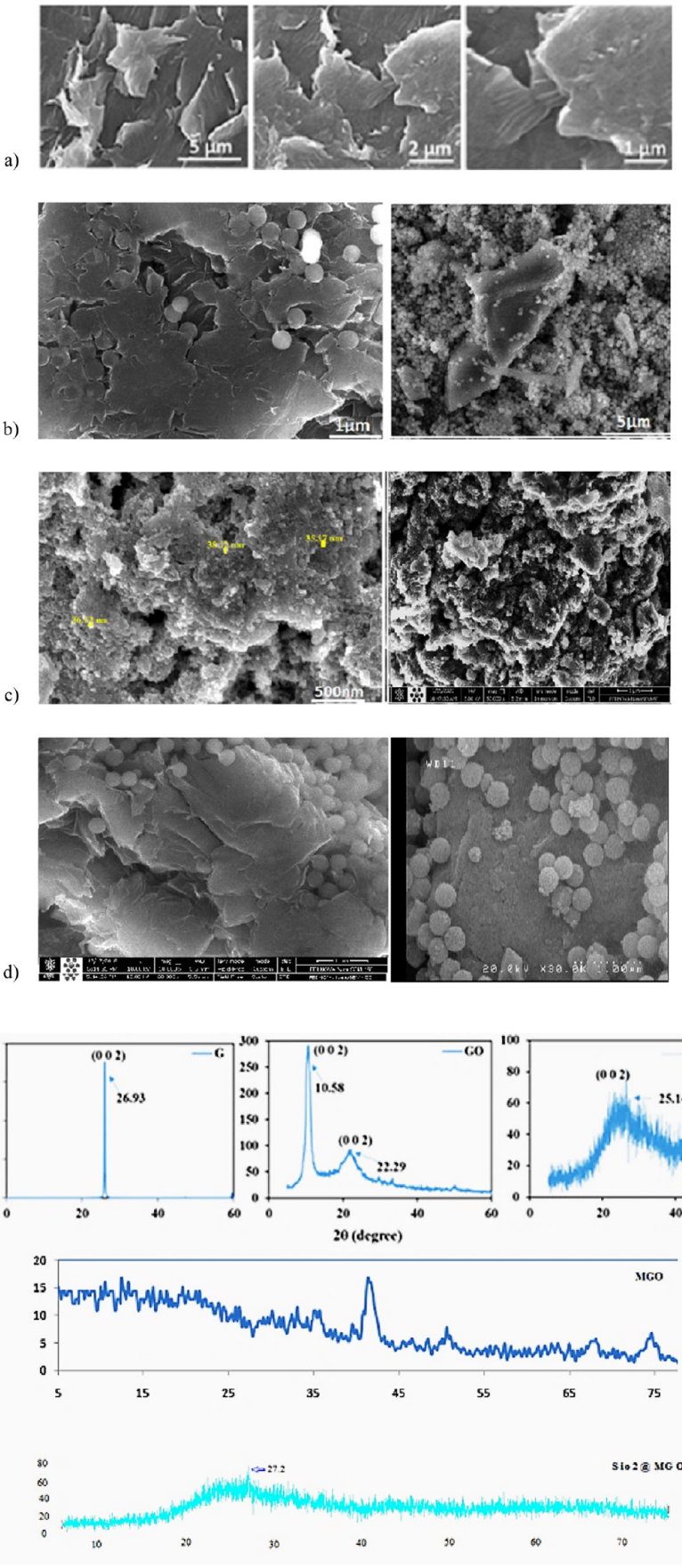

Figure 1. continued

https://doi.org/10.1021/acsomega.0c05395
ACS Omega 2021, 6, 21194−21206

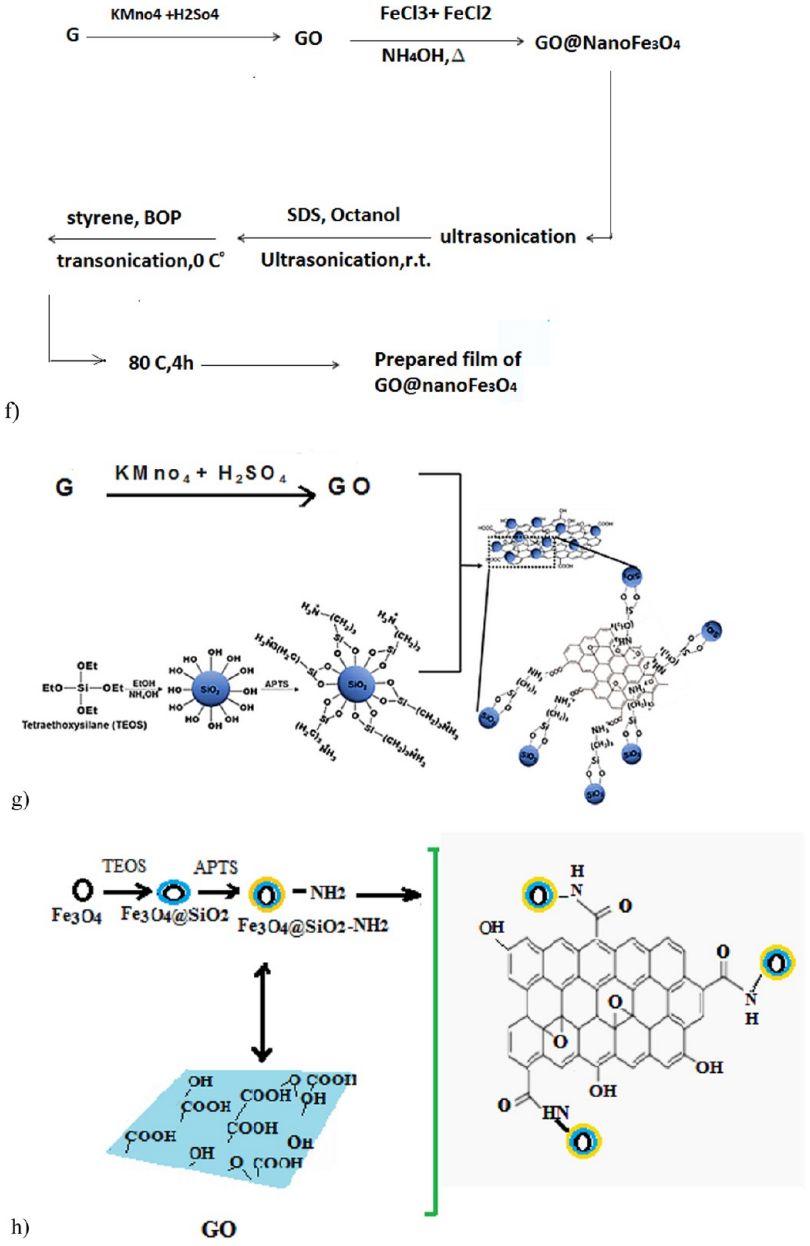

Figure 1. SEM images of (a) GO, (b) SGO, (c) Fe_3O_4 (left), SMGO, (right), and (d) MGO at different magnifications. XRD patterns of (e) pristine graphite powder, GO, SGO, MGO, and SMGO. Schematic representations of the synthesis of (f) MGO, (g) SGO, and (h) SMGO.

natural extracellular matrices, they are able to regulate the differentiation of stem cells.[24]

Graphene oxide (GO) as a new class of carbon nanomaterials is a derivative of graphene with a two-dimensional honeycomb structure. It appears to be biocompatible, with preferential affinity to the cell surface, and is less toxic than other carbon-based nanoparticles.[25] The main difference between graphene and GO is the controllable hydrophilic nature of GO, which makes it well-dispersible in water.[26] Because of its small size, ease of use, and large specific surface area,[27] GO has been recommended for biomedical applications such as biosensing,[28] drug/gene delivery,[29,30] and antibacterial effects.[31] In addition, GO can absorb surface factors including proteins and small molecules, which are the essential components for the differentiation of MSCs.[32,33] However, it is difficult to separate GO from the solution by conventional centrifugation and filtration methods as a result of its hydrophilicity, high dispersibility, and small size.[21]

Fe_3O_4 superparamagnetic nanoparticles are used in magnetically assisted drug delivery.[34] They can easily be separated by a magnetic field.[35−39] Nanocomposites based on magnetic GO (MGO) possess unique properties; they have a high specific surface area, surface-active sites, excellent magnetic characteristics, high chemical stability, an adjustable size and shape, and can be simply functionalized or modified.[26] However, because Fe_3O_4 only binds to the GO surface through electrostatic interaction or physical adsorption, it easily separates from the GO nanosheets during use. In addition, Fe_3O_4 easily oxidizes/dissolves when used in acidic solutions.[26,40,41] Therefore, a suitable structure, such as a silica shell, has been introduced.[26] Silica nanoparticles are biocompatible, have a unique morphology, and can be used as microcarriers.[42−44] They act as microcapsules that are easily loaded with the desired

https://doi.org/10.1021/acsomega.0c05395
ACS Omega 2021, 6, 21194−21206

therapeutic drug and can be delivered systemically or locally in a controlled manner.[45] The use of nanohybrid materials based on silica (silicon dioxide, SiO_2) can improve the biological and medical applications of GO. To enhance the functionality of GO for biological applications, it has been combined with Fe_3O_4 nanoparticles and silica as a biocompatible magnetic material.[34] Indeed, a silica-coated MGO can be synthesized, which is easy to disperse and contains a large number of active sites.[26]

In this study, we investigated whether the synthesized silica MGO (SMGO) increases the protective effects of MSC-CM in the treatment of liver damage in animal models. We studied the possible in vivo hepatoprotective effects of SMGO mixed with MSC-CM on the rat model of ALF induced by carbon tetrachloride (CCl_4). CCl_4 is a well-known hepatotoxin and is often used to induce ALF.[21] The ability of MSC-CM mixed with SMGO in the treatment of ALF in rats was analyzed by evaluating the serum level of enzymes and histopathological parameters.

RESULTS AND DISCUSSION

Synthesis of SMGO Nanohybrid. In this study, we developed a simple method for the synthesis of a SMGO nanohybrid and considered its intraperitoneal injection to improve the effect of MSC-CM on the treatment of CCl_4-induced liver damage in a rat model. Scanning electron microscopy (SEM) images of the as-prepared GO confirmed the synthesis of GO nanosheets with a quite smooth surface, where the distinctive layered structure of the sample was evident (Figure 1a–d). Spherical and uniform silica nanoparticles (particle size 100–200 nm) on the surface of GO nanosheets can be observed at different magnifications in the SEM images (Figure 1b). The dynamic light scattering (DLS) results of the SMGO (Figure 1e) were consistent with the SEM images and showed silica nanoparticles with a mean diameter of 155.2 nm and a low polydispersity index (PI = 2.5), indicating no aggregation in the solution. The binding of silica nanoparticles to two-dimensional (2D) GO nanosheets could, therefore, lead to the formation of the silica GO (SGO) nanohybrid, which effectively inhibited the aggregation of nanoparticles.[46] Schematic representations of the synthesis of SGO and SMGO and their characterization are shown in Figure 1f–h.

The structural properties of the pristine graphite powder and of the as-synthesized GO, MGO, SGO, and SMGO were analyzed and compared on the basis of their X-ray diffraction (XRD) patterns (Figure 1e). There were a sharp diffraction peak for the pristine graphite (2θ = 30.93°, index of 002, θ the Bragg angle) corresponding to a d-spacing of 0.334 nm. The as-prepared GO showed a characteristic peak at 2θ = 10.58°, which resulted from the diffraction on its 002 layer together with a broad diffraction peak at 22.29°, which was interpreted as a short-range order in stacked graphene sheets (Figure 1e).

Using the Debye–Scherrer equation, $L_a = 0.89\ \lambda/(\beta_{002} \cos \theta_{002})$, the number of graphene layers, n, in the as-synthesized GO sample was calculated as $n = L_a/d_{002} = 8$. Here, L_a, β, and d_{002} denote the stacking height, the full-width half-maxima, and the interlayer spacing, respectively,[47,48] and were obtained using the data from the XRD patterns. The MGO showed a broad peak at 2θ = 41.7°, whereas the SGO and SMGO had a broad peak at 2θ = 25.7 and 27.2°, respectively, indicating the presence of amorphous silica nanoparticles. In addition, the disappeared GO diffraction peak in the XRD pattern of the nanohybrid sample indicated that the stacking of the GO nanosheets in the hybrid structure was disordered.[49]

The zeta potential of the as-synthesized samples was determined after each step (Table 1). Because of their oxygenated functional groups, the GO nanosheets showed a negative potential of −50.8 mV above the surface. Conversely, the pristine amine-modified silica nanoparticles showed a positive potential of 40.0 mV, which indicated the grafting of $-NH_2$ groups on the surface of silica nanoparticles. The formation of SGO with a negative potential of −35.1 mV was due to the strong electrostatic interaction between the positively charged amine-modified silica nanoparticles and the negatively charged GO nanosheets (Table 1).[50] Accordingly, SMGO showed a positive potential of 11.2 mV due to its $-NH_2$ functional groups over oxygen. In addition, particle size distributions of amine-modified silica nanoparticles and the lateral dimensions of pristine GO nanosheets, SGO, MGO, and SMGO are also given in Table 1.

Table 1. Results for DLS and Zeta Potential for Pristine GO Nanosheets and Other Nanoparticles

sample	mean particle size (nm)	PDI	zeta potential (mV)
GO nanosheets	436.9	0.421	−50.8
amine-modified silica	378.7	0.533	40.0
SGO	155.2	0.227	−35.1
MGO	594	0.204	3.6
SMGO	647	0.101	11.2

The DLS results for the GO nanosheets showed that the lateral dimension of the sample was 436.9 nm, which is in agreement with previous studies.[51,52] In the case of amine-modified silica nanoparticles, the mean particle diameter was 378.7 nm, which was possibly due to the absence of a surfactant in their synthesis process and aggregation of nanoparticles.[53] However, the DLS results for SGO showed nanoparticles with a mean diameter of 155.2 nm, which indicated no aggregation in the solution. Therefore, the adhesion of silica nanoparticles to the 2D GO nanosheets could lead to the formation of SGO, which effectively inhibited the aggregation of nanoparticles.[46] The DLS results for MGO and SMGO showed the mean diameter of 594 and 647 nm, respectively (Table 1).

Finally, the results for the XRD, SEM, DLS, and Zeta potential confirmed the formation of a hybrid structure of SGO in which the silica nanoparticles were successfully bonded to the surface of GO and densely covered its surface. Such a special structure together with numerous hydroxyl group (OH) functionalities on the surface of nanohybrid explained the redispersibility of the sample in water readily using mild ultrasonication. The GO nanosheets provided a platform with active oxygenated functional groups to electrostatically stabilize the positively charge modified silica nanoparticles on its surface. The elemental composition of GO nanosheets, SGO, MGO, and SMGO were determined using energy-dispersive X-ray spectroscopy (EDX) analysis and the results are given in Table 2.

SMGO Inhibits the Release of Liver Enzymes and Improves the Survival Rate. Following the CCl_4-induced liver damage, liver models easily succumb to hepatocyte apoptosis and inflammatory responses. We showed in this study that the intraperitoneal injection of MSC-CM together

https://doi.org/10.1021/acsomega.0c05395
ACS Omega 2021, 6, 21194–21206

Table 2. EDX Results for Pristine GO Nanosheets and the Other Nanohybrids

sample	C (wt %)	O (wt %)	Si (wt %)	O/C	Si/C	Fe
GO nanosheets	52.43	47.12		0.89		
SGO	66.92	25.45	7.63	0.38	0.11	
MGO	21.00	38.83		1.75		42.17
SMGO	9.49	56.19	27.90	5.9	2.9	6.42

with SMGO resulted in reduced damage and rapid regeneration of liver cells. A significant survival benefit was also observed in the rats examined. Our results indicated that treatment with SMGO significantly improved the survival rate of CCl_4-induced liver failure in rats that received MSC-CM (Figure 2a). While only 20% of the rats survived for 35 days in the CCl_4 group, 60 and 57% survived in the MSC-CM and SMGO groups, respectively, and 100% survived during this period in the MSC-CM + SMGO group. Liver damage was reduced in both MSC-CM and MSC-CM + SMGO groups compared to the CCl_4 group 96 h after the injection. The recipients of MSC-CM + SMGO developed liver dysfunction with significantly lower alanine aminotransferase (ALT), aspartate aminotransferase (AST), and alkaline phosphatase (ALP) liver enzyme levels compared to the groups that received either MSC-CM or SMGO (Figure 2b–d). Therefore, intraperitoneal injection of MSC-CM + SMGO provided a significant survival benefit as it helped protect against liver damage and reduce mortality in recipient animals.

Lotfinia et al. reported, however, that while MSC-CM and ESC-MSC improved liver function, they did not increase survival.[16] According to Du et al., MSC-CM prevented the release of liver damage biomarkers and provided a significant survival benefit by inhibiting hepatocellular death and stimulating regeneration.[6] They reported a 7 day survival of 90% in the damaged livers treated with MSC-CM. However,

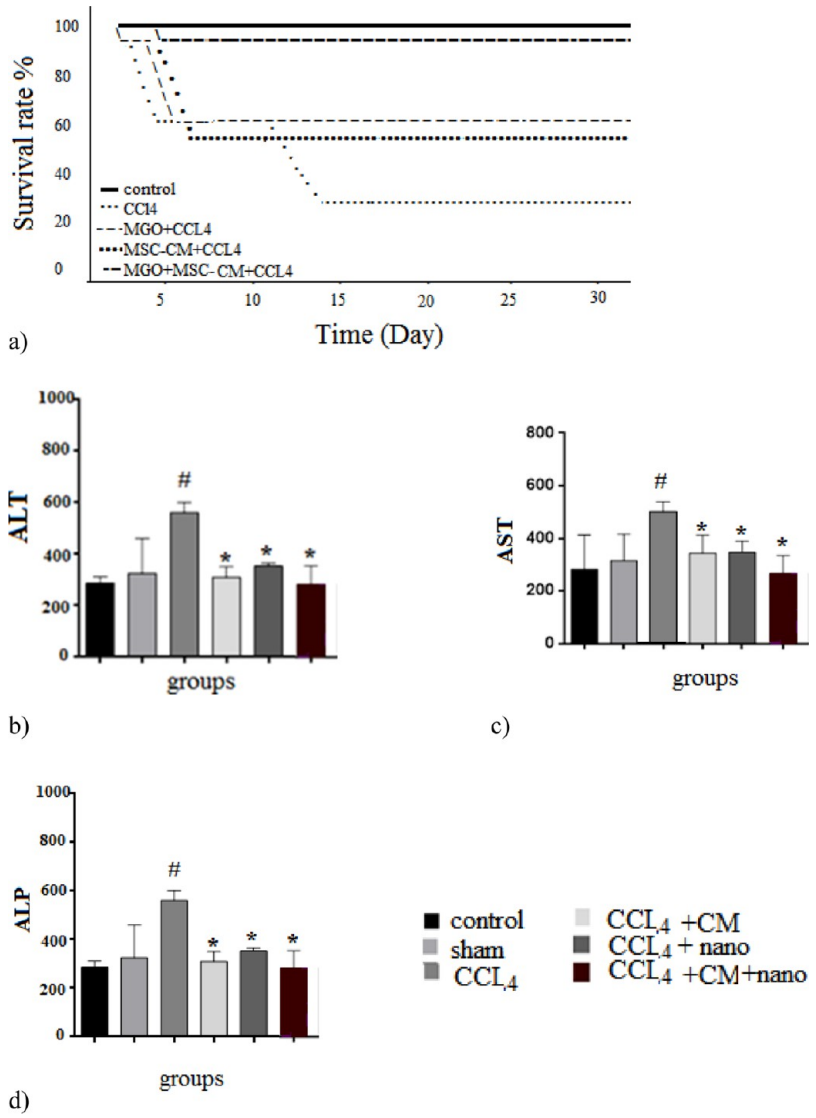

Figure 2. Treatment with SMGO increased (a) the survival rate, and decreased (b) AST, (c) ALT, and (d) ALP serum levels of CCl_4-induced acute liver damage in rats collected 96 h after treatment (n = 5, *P < 0.05, #P < 0.01). Here, nano refers to SMGO. Data are presented as mean ± SD. (*) and (#) indicate differences from the CCl_4 and control groups respectively, as determined by ANOVA with Tukey's HSD test. ALT: alanine aminotransferase, AST: aspartate aminotransferase, ALP: alkaline phosphatase, CCl_4: carbon tetrachloride. Abbreviations: CM, conditioned medium; CCL_4, carbon tetrachloride; and SMGO, silica magnetic graphene oxide.

https://doi.org/10.1021/acsomega.0c05395
ACS Omega 2021, 6, 21194–21206

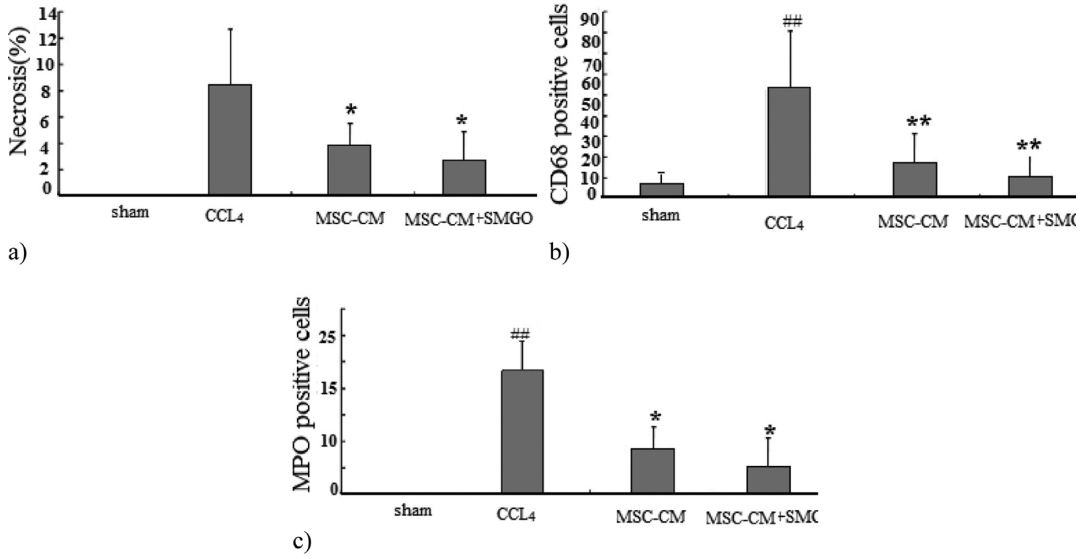

Figure 3. (a) Liver cell necrosis was quantified in the sham, CCl_4, MSC-CM, and MSC-CM + SMGO groups. Treatment with SMGO reduced infiltration of neutrophils and activation of Kupffer cells; (b) Kupffer cell activation was assessed by labeling CD68 in sections 96 h after operation; and (c) neutrophil infiltration was visualized by MPO immunostaining in sections 96 h after operation. *P < 0.05, **P < 0.01; ##P < 0.01. Abbreviations: CM, conditioned medium; CCl_4, carbon tetrachloride; and SMGO, silica magnetic graphene oxide.

we showed in this study that the 7 day survival in the MSC-CM + SMGO group was 100%, leading to the conclusion that SMGO increased the beneficial effects of MSC-CM on the treatment of damaged livers. Nevertheless, further studies are required to determine the mechanism involved.

SMGO Injection Improves Histopathologic Appearance and Reduces Neutrophil and Kupffer Cell Infiltration. We also examined the histopathologic changes in H&E and immunostained liver sections (Figures 4−7, Table 3). In the CCl_4 group, a significant increase in the number of neutrophil and Kupffer cells was found and compared to the control group. However, only a slight infiltration of inflammatory cell was observed in the MSC-CM + SMGO group compared to the MSC-CM and SMGO groups (Figures 4−7). The results indicated a significant reduction in the number of neutrophil and Kupffer cell infiltrations in the MGO and MSC-CM groups compared to the CCl_4 group (P < 0.01) (Figures 3 and 5). In other words, the number of these cells in the MSC-CM + SMGO group was lower than that in the SMGO and MSC-CM groups (P < 0.01) (Figure 3a). The number of CD68 cells was also significantly lower in the MSC-CM + SMGO group compared to other groups (Figure 3b). MPO-positive cells were also evident in all groups, however, the number of MPO-positive cells was significantly lower in the CCl_4 group after treatment with MSC-CM and MGO (P < 0.05) (Figure 3c). Treatment with SMGO reduced the number of CD68 and MPO-positive cells in the CCl_4MSC-CM group significantly (P < 0.01). The results indicated that SMGO improved the effects of MSC-CM on the treatment of damaged liver.

Our results suggest that, similar to MSC-CM, SMGO prevents immune cells from invading and/or functioning in the damaged liver. Decreased apoptosis of hepatocytes after treatment with MSC-CM + SMGO may be due in part to a decrease in proinflammatory cytokine levels, including IL-6, TNF-α, neutrophil infiltration, and Kupffer cell activation. In addition, MSC-CM + SMGO may inhibit immune cells to function in the damaged liver. SMGO + MSC-CM not only inhibited the apoptosis of hepatocytes, but also promoted their regeneration. This was accompanied by a significant reduction in neutrophil infiltration and the activation of Kupffer cells, as well as a marked reduction in the expression levels of proinflammatory cytokines such as TNF-α, IL-6, and CD68. MPO-positive cells were also present in liver tissue induced by CCl_4 and MSC-CM groups, but the number of these cells was significantly lower after SMGO injection. However, little inflammatory cell infiltration was observed in the SMGO and SMGO + MSC-CM groups. The results showed that MSC-CM reduced necrosis of the damaged liver (Figure 3).

SMGO Lowers the Level of Proinflammatory Cytokines and Increases the Expression of Vascular Endothelial Growth Factor and MMP-9 in Damaged Livers. In the CCl_4-induced livers, the expression levels of proinflammatory cytokines such as TNF-α, IL-6, and Caspase-3 decreased after SMGO injection. Damaged livers stained with TNF-α, IL-6, and Caspase-3 antibodies showed that SMGO injection inhibited apoptosis and necrosis of hepatocytes. Many apoptotic hepatocyte nuclei were observed in the CCl_4 group. Therefore, SMGO promotes the survival of hepatocytes in the CCl_4 group. The necrosis of the damaged liver in the SMGO + MSC-CM group was lower than that in the MSC-CM group. Treatment with SMGO + MSC-CM reduced the local expression of the proinflammatory cytokine TNF-α. In addition, it reduced proinflammatory cytokine IL-6 and Caspase-3 levels in CCl_4-induced liver damage compared to treatment with either SMGO or MSC-CM. The results confirmed the role of graphene-based materials in reducing apoptosis. Several studies have shown direct antiapoptotic effects of MSC-CM on hepatocytes.[6] MSC-CM provides trophic support to the damaged liver by inhibiting hepatocyte death and inducing regeneration, and has direct promitosis effects on hepatocytes and increases the hepatic expression of cytokines and growth factors that are relevant for cell angiogenesis, proliferation, and anti-inflammatory responses.[6] In our study, fewer apoptotic hepatocytes were observed after the injection of MSC-CM + SMGO compared to MSC-CM

https://doi.org/10.1021/acsomega.0c05395
ACS Omega 2021, 6, 21194−21206

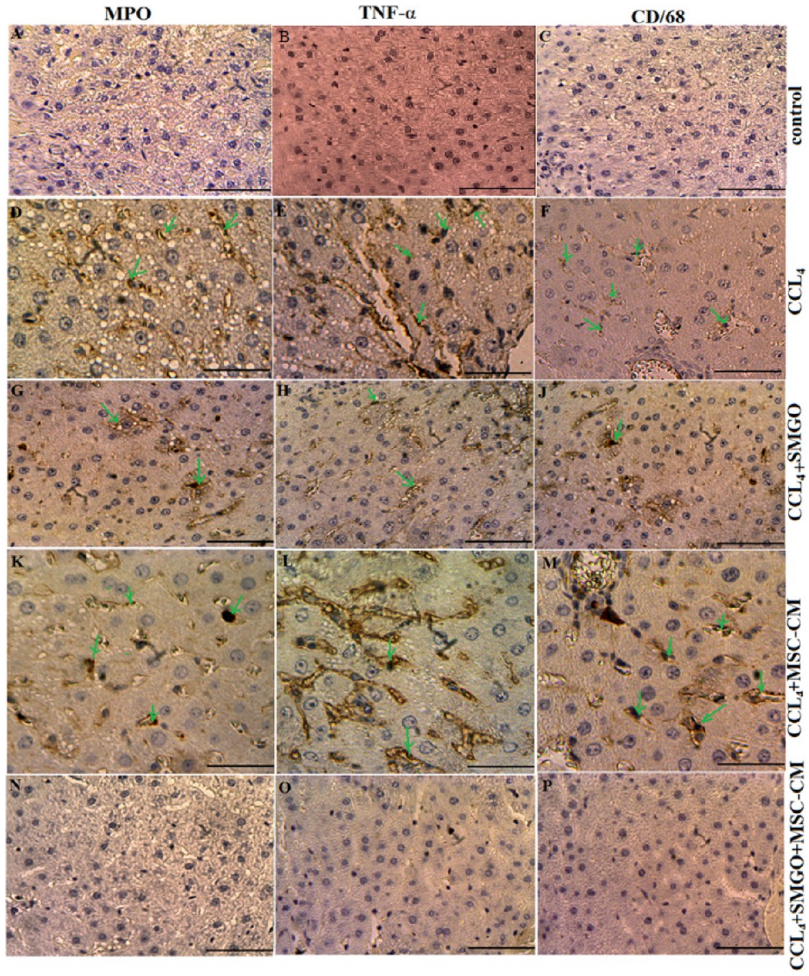

Figure 4. Treatment with MSC-CM mixed with SMGO improved microscopic histopathologic parameters of CCl_4-induced liver damage and reduced infiltration of neutrophils (A,D,G,K,N), proinflammatory cytokine TNF-α (B,E,H,L,O), and activation of Kupffer cells (C,F,J,M,P). Liver samples taken 4 days after the injection of CCl_4, CCl_4 + SMGO, CCl_4 + MSC-CM, and CCl_4 + MSC-CM + SMGO subject to immunohistologic analysis. Neutrophil, necrosis, and Kupffer cell were stained by labeling MPO, TNF-α, and CD68, respectively, in liver sections. Arrows mark MPO +, TNF-α+, and CD68+ cells. Scale bars, 200 μm (A−C,G,H,J,N−P) and 400 μm (D−F,K−M). Abbreviations: CM, conditioned medium; CCl_4, carbon tetrachloride; and SMGO, silica magnetic graphene oxide.

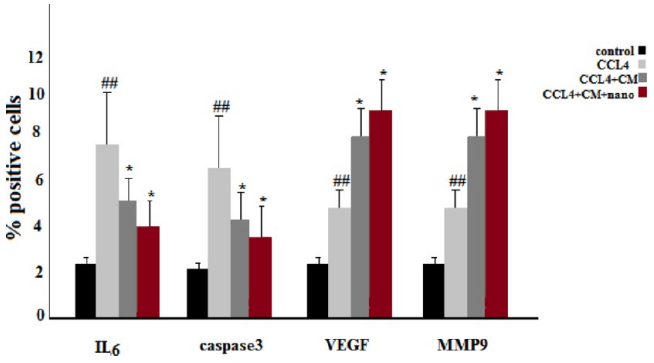

Figure 5. Number of IL-6 and Caspase-3 positive cells was significantly lower in the MSC-CM and MSC-CM + SMGO groups compared to that in the CCl_4 group. Here, nano refers to SMGO. The number of VEGF and MMP-9 positive cells was significantly higher in the MSC-CM and MSC-CM + SMGO groups compared to that in the CCl_4 group (*P < 0.05, ##P < 0.01). Abbreviations: CM, conditioned medium; CCl_4, carbon tetrachloride; and SMGO, silica magnetic graphene oxide.

alone. We showed that MSC-CM mixed with SMGO prevented apoptosis of liver cells through the secretion of vascular endothelial growth factor (VEGF) in vivo. We also showed that the expression of VEGF and MMP-9 was significantly upregulated 72 h after the injection of the medium-mixed nanomaterial. Moreover, higher VEGF and MMP-9 levels were accompanied by hepatocytes and their proliferation after treatment. VEGF as a trophic factor is an important mediator of immune tolerance in the damaged tissue microenvironment and can induce the growth, proliferation, and neovascularization of hepatocytes *in vivo*.[6,16]

The levels of these cytokines were lower in the MSC-CM + SMGO group than in the SMGO and MSC-CM groups. Moreover, the expression of VEGF and MMP-9 was significantly upregulated after treatment with SMGO (Figures 5 and 6). MMP9 also plays a dual role in the damaged liver. MMP-9 overexpression is significantly correlated with liver injury in the early stages after injury, possibly through the upregulation of proinflammatory cytokines, which mediate leukocyte migration and apoptotic pathways.[6] However, MMP9 is also important for liver regeneration beyond angiogenesis and matrix remodeling. The mechanism is likely to be through the overexpression of hepatocyte growth factor,

https://doi.org/10.1021/acsomega.0c05395
ACS Omega 2021, 6, 21194−21206

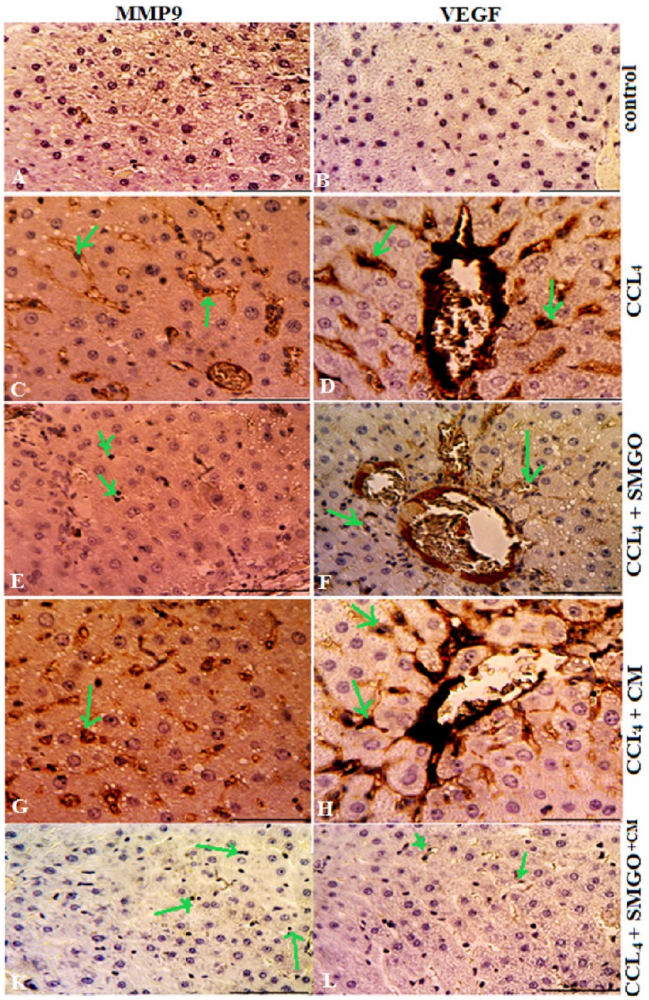

Figure 6. Effects of SMGO on the expression of VEGF and MMP-9 in the damaged livers treated with MSC-CM. MGO enhanced the number of VEGF and MMP-9-positive cells in the CCl_4-induced livers treated with MSC-CM. Positive cells were visualized by VEGF and MMP-9 immunostaining in the liver sections 4 days after the injection. Scale bar, 200 μm (control, CCl_4 + SMGO, and CCl_4 + CM + SMGO); Scale bar, 400 μm (CCl_4, CCl_4 + CM). Arrows mark MMP9+ and VEGF + cells. Scale bars, 200 μm (A,B,E,F,K,L) and 400 μm (C,D,G,H). Abbreviations: CM, conditioned medium; CCl_4, carbon tetrachloride; and SMGO, silica magnetic graphene oxide.

VEGF, TNF, and/or altered regulation of both proliferative and apoptotic pathways.[54] In our study, upregulation of MMP9 expression occurs 96 h after SMGO and MSC-CM therapy. During this time, the level of regeneration was higher than the level of injury, so we have reason to believe that overexpression of MMP9 is beneficial to liver regeneration. MMP-9 is essential for liver regeneration beyond angiogenesis and matrix remodeling. Its mechanism is presumably based on the upregulation of the hepatocyte growth factor TNF-α, VEGF, and/or an altered regulation of both proliferative and apoptotic signaling pathways.[54] Because the addition of SMGO to MSC-CM decreased the number of apoptotic cells, we propose that SMGO upregulates the expression of VEGF and promotes the rapid proliferation of hepatocytes and the regeneration of the damaged liver as an essential factor in restoring liver function after injury.[6]

Also, the ELISA results showed a higher level of VEGF in SMGO + MSC-CM compared with the CCl_4 group. On the other hand, higher levels of VEGF were found in SMGO + MSC-CM compared with SMGO and MSC-CM groups (Figure 8). The ELISA results showed a higher level of VEGF in SMGO + MSC-CM compared with the CCl_4 group. TNF-α and IL-6 expressions were lower in the serum of rats receiving SMGO compared with the MSC-CM group (Figure 8).

Because MSCs influence models of ALF primarily through paracrine or endocrine mechanisms rather than direct differentiation, adding some factors to the conditioning medium can increase the therapeutic effects of stem cells. Using SMGO was an effective way to improve the therapeutic effects of stem cells. In this study, the increased therapeutic effects of MSC-CM on the damaged liver may be due to the unique physiochemical properties of SMGO. It also appeared that the better effectiveness of MSC-CM in treating the damaged liver was due to the improved delivery of growth factors within the medium to the tissues.

GO exhibits efficient internalization within the cells,[9,55−57] and has a large surface area for functionalization and superior mechanical properties,[33] which makes it attractive for tissue engineering and drug delivery.[58−62] On the other hand, it has been reported that it can induce spontaneous differentiation of MSCs without extrinsic biochemical manipulation.[63,64] This enables it to act as a potential candidate for the delivery of growth factors to the damaged tissue in vivo. Superparamagnetic iron oxide nanoparticles are used in magnetically assisted drug delivery,[65,66] and the drug transport property of MGO is achieved through the noncovalent binding of the drug to GO.

As a platform for drug delivery, MGO has shown successful fluorescence-tracked transport of hydrophobic doxorubicin noncovalently conjugated to GO with improved efficacy.[34] MGO is mainly used to remove pollutants such as heavy metals or organic molecules through magnetic separation or in lithium ion batteries.[46] Because Fe_3O_4 offers superparamagnetic properties for magnetic targeted drug delivery, which allow easy manipulation by the magnetic field,[34] it plays an important role in the higher binding capacity of GO to biomolecules within MSC-CM. In this work, we synthesized SMGO and examined its role in increasing proliferation and angiogenesis, and decreasing apoptosis in the damaged liver cells through the ability to binding and then release growth factors. For this reason, we proposed SMGO nanoparticles as a novel multifunctional magnetic target platform for the highly effective delivery of biomolecules capable of treating damaged liver in vivo. We showed that GO combined with Fe_3O_4 and silica nanoparticles as a biocompatible magnetic material accelerates growth factor delivery to damaged tissue.

CONCLUSIONS

Our results indicated that SMGO improved the effects of MSC-CM on the treatment of CCl_4-induced damaged livers. It inhibited liver parenchymal cell death and improved its regeneration through trophic support, thereby improving the survival rate. In addition to stem cell therapy, stem cell modifications or MSCs in combination with other treatment methods are increasingly being considered. We concluded that in addition to transplanting MSC-CM, liver damage can be synergistically treated with SMGO through preventing apoptosis, enhancing angiogenesis, and/or blocking the action of inflammatory factors. The intraperitoneal injection of MSC-CM + SMGO causes an increased expression of cytokines in

https://doi.org/10.1021/acsomega.0c05395
ACS Omega 2021, 6, 21194−21206

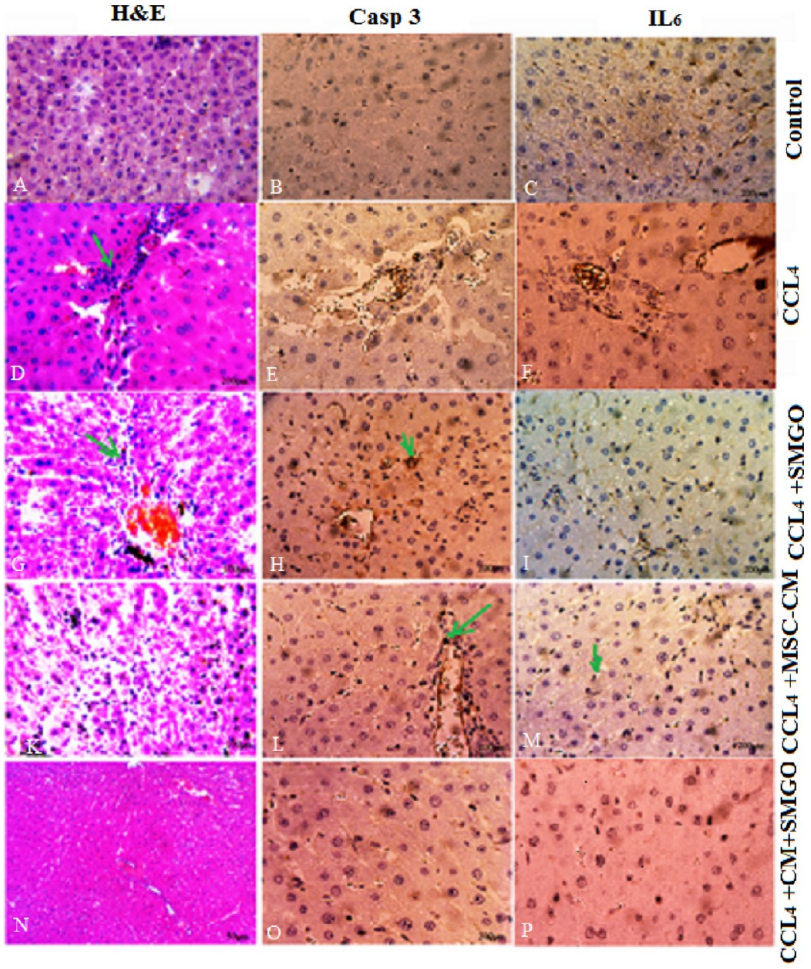

Figure 7. Treatment with MSC-CM + SMGO after 3 days decreased the levels of proinflammatory cytokines IL-6 and Caspase-3 in liver failure induced by CCl_4 compared to treatment with either SMGO or MSC-CM. Sections stained with H&E, IL-6, and Caspase-3. Abbreviations: CM, conditioned medium; CCl_4, carbon tetrachloride; and SMGO, silica magnetic graphene oxide. Arrows mark inflammatory (H&E), Casp3+, and IL6+ cells. Scale bars, 200 μm (A−C,H,G,N−P) and 400 μm (D−F,K−M).

Table 3. Microscopic Evaluation of Hepatocytes in Different Treatment Groups[a]

sample	average apoptotic cells per field	% apoptosis	accumulation of inflammatory cells	hyperemia
control	−	0	−	−
sham	−	0	−	−
CCl_4	62	17.71	+++	+++
SMGO	20	5.70	++	++
MSC-CM	33	9.42	+	+
MSC-CM + SMGO	6	1.71	++	++

[a]Treatment with SMGO improved the effects of MSC-CM on histopathologic appearance. −, +, ++, and +++ were used to assess hyperemia and accumulation of inflammatory cells and indicate no effect, slight, mild, and intensive, respectively.

the regenerating liver, presumably by activating an endogenous pathway. Further studies are required to determine the exact mechanism.

EXPERIMENTAL SECTION

Natural flake graphite powder was obtained from Qingdao graphite Co., China. Sulfuric acid (H_2SO_4) 98%, hydrogen peroxide (H_2O_2) 30%, hydrogen chloride (HCl) 37%, potassium permanganate ($KMnO_4$), tetraethyl orthosilicate (TEOS), 3-aminopropyltrimethoxysilane (APS) 97%, iron(III) trichloride hexahydrate ($FeCl_3{\cdot}6H_2O$), and iron dichloride tetrahydrate ($FeCl_2{\cdot}4H_2O$) were all supplied by Sigma-Aldrich Co., Germany. Carbon tetrachloride (CCl_4) was obtained from Merck chemicals, Germany.

Synthesis of the SGO Nanohybrid. The GO was synthesized according to the modified Hummer's method, which is based on oxidizing graphite powder by a strong oxidizing agent.[67] 0.5 g of graphite powder was placed in an ice bath in a round-bottom flask containing 50 mL of H_2SO_4 and 2 g of $KMnO_4$ was added gradually. The mixture was stirred for 2 h at a temperature below 10 °C and stirred for another 1 h at 35 °C. The reaction medium was diluted with 50 mL of distilled water in an ice bath, while maintaining the temperature below 100 °C, and stirred for an additional 1 h. The mixture was further diluted to 150 mL with distilled water.

https://doi.org/10.1021/acsomega.0c05395
ACS Omega 2021, 6, 21194−21206

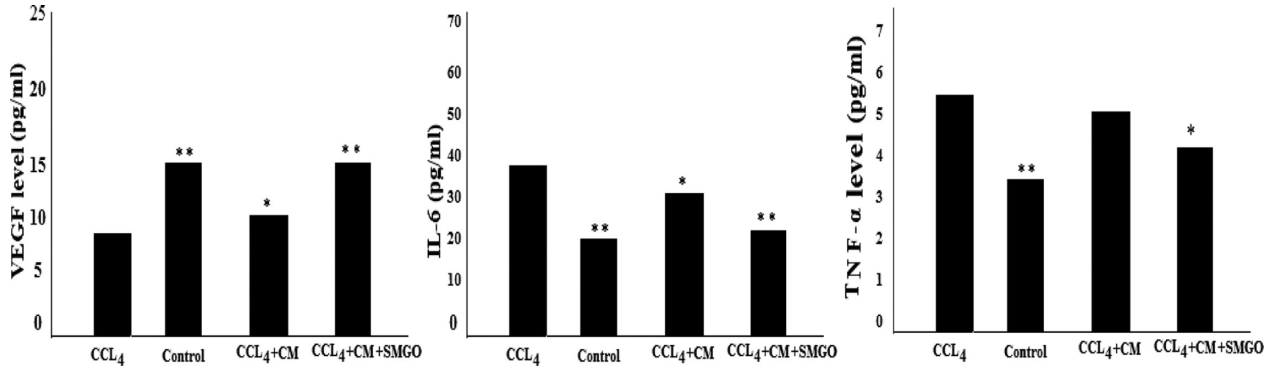

Figure 8. ELISA results of VEGF, IL-6, and TNF-α serum levels in CCl_4-induced rats receiving SMGO, MSC-CM, and SMGO + MSC-CM. Significant differences between the CCl_4 and the other groups were $^*P < 0/05$ and $^{**}P < 0.001$. Abbreviations: CM, conditioned medium; CCl_4, carbon tetrachloride; and SMGO, silica magnetic graphene oxide.

In order to eliminate the excess permanganate ion, 10 mL of H_2O_2 30% was added, whereby the color of the reaction mixture changed to bright yellow. The final product was centrifuged and washed three times with HCL 5%, followed by distilled water. The resulting solid was dried at 60 °C for 24 h.

Silica nanospheres were prepared using the Stöber method based on the sol−gel process.[68] 10 mL of TEOS was mixed with 32 mL of deionized water, 200 mL of ethanol, and 42.3 mL of ammonia solution at 70 °C. The solution was stirred for 30 min at 22 °C. Silica (SiO_2) nanoparticles were rinsed three times with ethanol and dried for 16 h. The surface modification of silica nanoparticles with the aminopropylsilane coupling agent was then carried out. 1 g of silica nanoparticles was mixed with 100 mL of alcohol/deionized water and 200 μL of aminopropylsilane for 12 h. SGO was then synthesized by the addition of dispersed GO (1 mg/mL) to the prepared amine-modified silica nanoparticles and the resulting mixture was stirred vigorously for 16 h.

Preparation of SMGO. SMGO was synthesized by the coprecipitation of ferric and ferrous chloride solutions ($FeCl_3 \cdot 6H_2O$, and $FeCl_2 \cdot 4H_2O$, respectively) in the presence of the SGO. The solutions were prepared at a 2:1 mole ratio. The sample was prepared through a sonication method, in which the separately synthesized Fe_3O_4 nanoparticles and SGO were dispersed in an ultrasonic bath. The resulting mixture was homogenized, centrifuged, and dried at 60 °C.

Characterization of SMGO. The as-synthesized samples were characterized using XRD (Philips Xpert MPD Co., K-irradiation 1.78897 Å), SEM (Philips XL30 microscope, accelerating voltage 25 kV), and dynamic light scattering (DLS, Horiba SZ-100).

Animals and Experimental Design. Syngeneic male Sprague−Dawley rats (220−280 g, Royan Institute, Iran) were kept under standard conditions in a light environment with temperature and humidity control. This study was approved by the Animal Care and Use Committee of the School of Biological Sciences at Kharazmi University, Iran. The acute liver damage model was obtained using a single intraperitoneal injection of 2 mL/kg body weight of CCl_4 dissolved in sterile olive oil (1:1). To produce MSC-CM, passage-3 MSC cells were grown to 80% confluence cultured in a Dulbecco's modified eagle's medium supplemented with bovine serum albumin. MSC-CM was collected after 10 h.

The rats were divided into six groups, namely, a control group receiving no treatment, a sham group injected with only olive oil, a group injected with CCl_4, a group injected with CCl_4 and 400 μL MSC-CM of 5×10^6 cells, a group injected with CCl_4 and 300 μg/kg body weight of SMGO, and a group injected with CCl_4, MSC-CM, and 300 μg/kg body weight of SMGO. All injections were intraperitoneal. For the sake of brevity, we refer to these groups as control, sham, CCl_4, MSC-CM, SMGO, and MSC-CM + SMGO, respectively.

The number of rats in each group was $n = 6$. All animals received treatment on the first day. They were anesthetized with ether 4 days after the intraperitoneal injection of CCl_4, MSC-CM, and 300 μg/kg body weight of SMGO. Blood samples were collected from the heart for biochemical analysis and the livers were then taken for histological and immunostaining examination.

Quantification of Serum Biochemical. The blood samples were kept at room temperature for 1 h and then centrifuged at 1500g for 12 min at 4 °C. The serum was separated and kept at 20 °C until analysis. Serum levels of ALT, AST, and ALP were measured using an automated analyzer (Hitachi, Japan) and commercially available kits (Pars Azmun, Iran) according to the manufacturer's instructions.

Liver Histology and Immunohistology. The liver tissues were stained with hematoxylin and eosin (H&E) and observed with a light microscope (Zeiss, Germany). Primary mouse antibodies anti-MPO (1/100; Abcam, Cambridge, UK), the anti-CD68 monoclonal antibody (1:200; Serotec, Oxford, UK), anti-MMP-9, and anti-VEGF were used to target neutrophils, Kupffer cells, and liver regeneration-related proteins, respectively. Anti-TNF-α, anti-Caspase-3, and anti-IL-6 were also used to identify apoptosis and proinflammatory cytokines.

VEGF, TNF-α, and IL-6 Enzyme-Linked Immunosorbent Assay. Serum levels of VEGF, TNF-α, and IL-6 were measured by the enzyme-linked immunosorbent assay (ELISA) method. They were measured with ELISA Kits Rat VEGF (RRV00; R&D; USA; Inc), Rat TNF-α (Dy510; R&D; USA; Inc), and Rat IL-6 (R6000B; R7D; USA; Inc).

Statistical Analysis. The data were analyzed using one-way analysis of variance for multiple comparisons. The significance level was set at $P < 0.05$ and $P < 0.01$. All data are expressed as means ± SE. The Kolmogorov−Smirnov test was used to study the normal distribution. Parametric continuous data with normal distribution between different groups were compared by one-way analysis of variance (ANOVA), followed by post hoc and Tukey tests.

https://doi.org/10.1021/acsomega.0c05395
ACS Omega 2021, 6, 21194−21206

AUTHOR INFORMATION

Corresponding Author

Tahereh Foroutan − *Department of Animal Biology, Faculty of Biological Sciences, Kharazmi University, Tehran 15614, Iran;* orcid.org/0000-0002-1476-3928; Email: Foroutan@khu.ac.ir

Authors

Fahimeh Kabiri − *Department of Animal Biology, Faculty of Biological Sciences, Kharazmi University, Tehran 15614, Iran*

Elaheh Motamedi − *Department of Nanotechnology, Agricultural Biotechnology Research Institute of Iran (ABRII), Agricultural Research, Education and Extension Organization (AREEO), Karaj 3173655111, Iran;* orcid.org/0000-0001-6324-2291

Complete contact information is available at: https://pubs.acs.org/10.1021/acsomega.0c05395

Author Contributions

T.F. performed the investigation and formal analysis and wrote the original draft. F.K. and E.M. carried out the investigation and formal analysis.

Notes

The authors declare no competing financial interest.

ACKNOWLEDGMENTS

The authors express their great appreciation to the anonymous reviewers for their valuable time, constructive comments, and helpful suggestions.

REFERENCES

(1) Fu, Y.; Zheng, S.; Lin, J.; Ryerse, J.; Chen, A. Curcumin protects the rat liver from CCl_4-caused injury and fibrogenesis by attenuating oxidative stress and suppressing inflammation. *Mol. Pharmacol.* **2008**, *73*, 399−409.

(2) Wang, Y.-H.; Wu, D.-B.; Chen, B.; Chen, E.-Q.; Tang, H. Progress in mesenchymal stem cell−based therapy for acute liver failure. *Stem Cell Res. Ther.* **2018**, *9*, 227.

(3) Saliba, F.; Samuel, D. Acute liver failure, current trends. *J. Hepatol.* **2013**, *59*, 6−8.

(4) Volarevic, V.; Nurkovic, J.; Arsenijevic, N.; Stojkovic, M. Concise review, therapeutic potential of mesenchymal stem cells for the treatment of acute liver failure and cirrhosis. *Stem Cells* **2014**, *32*, 2818−2823.

(5) Tao, Y.-C.; Wang, M.-L.; Chen, E.-Q.; Tang, H. Stem cells transplantation in the treatment of patients with liver failure. *Curr. Stem Cell Res. Ther.* **2018**, *13*, 193−201.

(6) Du, Z.; Wei, C.; Cheng, K.; Han, B.; Yan, J.; Zhang, M.; Peng, C.; Liu, Y. Mesenchymal stem cell conditioned medium reduces liver injury and enhances regeneration in reduced-size rat liver transplantation. *J. Surg. Res.* **2013**, *183*, 907−915.

(7) Kopp, J. L.; Grompe, M.; Sander, M. Stem cells versus plasticity in liver and pancreas regeneration. *Nat. Cell Biol.* **2016**, *18*, 238−245.

(8) Li, N.; Zhang, Q.; Gao, S.; Song, Q.; Huang, R.; Wang, L.; Liu, L.; Dai, J.; Tang, M.; Cheng, G. Three-dimensional graphene foam as a biocompatible and conductive scaffold for neural stem cells. *Sci. Rep.* **2013**, *3*, 1604.

(9) Solanki, A.; Chueng, S. T.; Yin, P. T.; Kappera, TR.; Chhowalla, M.; Lee, K. B. Axonal alignment and enhanced neuronal differentiation of neural stem cells on graphene-nanoparticle hybrid structures. *Adv. Mater.* **2013**, *25*, 5477.

(10) Nayak, T. R.; Andersen, H.; Makam, V. S.; Khaw, C.; Bae, S.; Xu, X.; Ee, P.-L. R.; Ahn, J.-H.; Hong, B. H.; Pastorin, G.; Özyilmaz, B. Graphene for controlled and accelerated osteogenic differentiation of human mesenchymal stem cells. *ACS Nano* **2011**, *5*, 4670.

(11) Neve, R. L.; Harris, P.; Kosik, K. S.; Kurnit, D. M.; Donlon, T. A. Identification of cDNA clones for the human microtubule-associated protein tau and chromosomal localization of the genes for tau and microtubule-associated protein. *Brain Res.* **1986**, *1*, 271−280.

(12) Lin, F.; Moran, A.; Igarashi, P. Intra renal cells not bone marrow-derived cells, are the major source for regeneration in postischemic kidney. *J. Clin. Invest.* **2005**, *115*, 1756−1764.

(13) Lin, F.; Cordes, K.; Li, L.; Hood, L.; Couser, W. G.; Shankland, S. J.; Igarashi, P. Hematopoietic stem cells contribute to the regeneration of renal tubules after renal ischemia-reperfusion injury in mice. *J. Am. Soc. Nephrol.* **2003**, *14*, 1188−1199.

(14) Park, J.; Kim, B.; Han, J.; Oh, J.; Park, S.; Ryu, S.; Jung, S.; Shin, J.-Y.; Lee, B. S.; Hong, B. H.; Choi, D.; Kim, B.-S. Graphene oxide flakes as a cellular adhesive, Prevention of reactive oxygen species mediated death of implanted cells for cardiac repair. *ACS Nano* **2015**, *9*, 4987−4999.

(15) Abedi, A.; Azarnia, M.; Jamali Zahvarehy, M.; Foroutan, T.; Golestani, S. Effect of different times of intraperitoneal injections of human bone marrow mesenchymal stem cell conditioned medium on gentamicin-induced acute kidney injury. *Urol. J.* **2016**, *13*, 2707−2716.

(16) Lotfinia, M.; Kadivar, M.; Piryaei, A.; Pournasr, B.; Sardari, S.; Sodeifi, N.; Sayahpour, F.-A.; Baharvand, H. Effects of Secreted Molecules of Human Embryonic Stem Cell-Derived Mesenchymal Stem Cells on Acute Hepatic Failure Model. *Stem Cells Dev.* **2016**, *25*, 1898−1908.

(17) Eini, F.; Foroutan, T.; Bidadkosh, A.; Barin, A.; Dehghan, M. M.; Tajik, P. The effects of freeze/thawing process on cryopreserved equine umbilical cord blood-derived mesenchymal stem cells. *Comp. Clin. Pathol.* **2012**, *21*, 1713−1718.

(18) Abedini, F.; Foroutan, T.; Jahangiri, L. Alkaline phosphatase and CD34 reaction of deciduous teeth pulp stem cells. *Pak. J. Biol. Sci.* **2007**, *10*, 3146−3149.

(19) Ayobian-Markazi, N.; Fourootan, T.; Zahmatkesh, A. An in vitro evaluation of the responses of human osteoblast-like SaOs-2 cells to SLA titanium surfaces irradiated by erbium, yttrium−aluminum−garnet [Er, YAG] lasers. *Laser Med. Sci.* **2014**, *29*, 47−53.

(20) Foroutan, T.; Ahmadi, F.; Moayer, F.; Khalvati, S. Effects of intraperitoneal injection of magnetic graphene oxide on the improvement of acute liver injury induced by CCL4. *Biomater. Res.* **2020**, *24*, 14.

(21) Foroutan, T.; Amid, A.; Karimi, M. R. Comparison of manual tools, ultrasonic and erbium-doped yttrium aluminum garnet (Er: YAG) laser on the debridement effect of the surface of the root of teeth suffering from. *J. Laser Med. Sci.* **2013**, *4*, 199.

(22) Foroutan, T.; Nazemi, N.; Tavana, M.; Kassaee, M. Z.; Motamedi, E.; Sonieshargh, S.; zare Zardini, H. Suspended graphene oxide nanoparticle for accelerated multilayer osteoblast attachment. *J. Biomed. Mater. Res., Part A* **2018**, *106*, 293−303.

(23) Cruz, S.; Girão, A.; Gonçalves, G.; Marques, P. Graphene: The Missing Piece for Cancer Diagnosis? *Sensors* **2016**, *16*, 137.

(24) Kim, J.; Park, S.; Kim, Y. J.; Jeon, C. S.; Lim, K. T.; Seonwoo, H.; Chung, J. H. Monolayer graphene-directed growth and neuronal differentiation of mesenchymal stem cells. *J. Biomed. Nanotechnol.* **2015**, *11*, 2024.

(25) Szmidt, M.; Stankiewicz, A.; Urbańska, K.; Jaworski, S.; Kutwin, M.; Wierzbicki, M.; Grodzik, M.; Burzyńska, B.; Góra, M.; Chwalibog, A.; et al. Graphene oxide down-regulates genes of the oxidative phosphorylation complexes in a glioblastoma. *BMC Mol. Biol.* **2019**, *20*, 2.

(26) Suo, L.; Dong, X.; Gao, X.; Xu, J.; Huang, Z.; Ye, J.; Lu, X.; Zhao, L. Silica-coated magnetic graphene oxide nanocomposite based magnetic solid phase extraction of trace amounts of heavy metals in water samples prior to determination by inductively coupled plasma mass spectrometry. *Microchem. J.* **2019**, *149*, 104039.

(27) Gonçalves, G.; Vila, M.; Portolés, M.-T.; Vallet-Regi, M.; Gracio, J.; Marques, P. A. A. P. Nano-graphene oxide, a potential

multifunctional platform for cancer therapy. *Adv. Healthcare Mater.* **2013**, *2*, 1072−1090.
(28) Greenwel, P.; Domínguez-Rosales, J.-A.; Mavi, G.; Rivas-Estilla, A. M.; Rojkind, M. Hydrogen peroxide, a link between acetaldehyde-elicited alpha1[I] collagen gene up-regulation and oxidative stress in mouse hepatic stellate cells. *Hepatology* **2000**, *31*, 109−116.
(29) Lee, K. S.; Buck, M.; Houglum, K.; Chojkier, M. Activation of hepatic stellate cells by TGF alpha and collagen type I is mediated by oxidative stress through cmyb expression. *J. Clin. Invest.* **1995**, *96*, 2461−2468.
(30) Arthur, M. J.; Mann, D. A.; Iredale, J. P. Tissue inhibitors of metalloproteinases, hepatic stellate cells and liver fibrosis. *J. Gastroenterol. Hepatol.* **1998**, *13*, S33−S38.
(31) Benyon, R. C.; Arthur, M. J. P. Mechanisms of hepatic fibrosis. *J. Pediatr. Gastroenterol. Nutr.* **1998**, *27*, 75−85.
(32) Ryu, S.; Kim, B.-S. Culture of Neural Cells and Stem Cells on Graphene. *Tissue Eng. Regener. Med.* **2013**, *10*, 39.
(33) Yoon, H. H.; Bhang, S. H.; Kim, T.; Yu, T.; Hyeon, T.; Kim, B.-S. Dual Roles of Graphene Oxide in Chondrogenic differentiation of adult stem cells, cell-adhesion substrate and growth factor-delivery carrier. *Adv. Funct. Mater.* **2014**, *24*, 6455.
(34) Gonzalez-Rodriguez, R.; Campbell, E.; Naumov, A. Multifunctional graphene oxide/iron oxide nanoparticles for magnetic targeted drug delivery dual magnetic resonance/fluorescence imaging and cancer sensing. *PLoS One* **2019**, *6*, No. e0217072.
(35) Amirhassan, A.; Mehdi, B.; Eliye, H. Poly [pyrrole-co-aniline] @graphene oxide/Fe3O4 sorbent for the extraction and preconcentration of polycyclic aromatic hydrocarbons from water samples. *New J. Chem.* **2018**, *42*, 16744−16751.
(36) Liu, M.; Wen, T.; Wu, X.; Chen, C.; Hu, J.; Li, J.; Wang, X. Synthesis of porous Fe3O4 hollow microspheres/graphene oxide composite for Cr [VI] removal. *Dalton Trans.* **2013**, *42*, 14710−14717.
(37) Yang, S.; Zong, P.; Ren, X.; et al. Rapid and highly efficient preconcentration of Eu [III] by core-shell structured Fe3O4@ humic acid magnetic nanoparticles. *ACS Appl. Mater. Interfaces* **2012**, *4*, 6891−6900.
(38) Liao, N.; Liu, Z.; Zhang, W.; Gong, S.; Ren, D.; Ke, L.; Lin, K.; Yang, H.; He, F.; Jiang, H. Preparation of a novel Fe3O4/graphene oxide hybrid for adsorptive removal of methylene blue from water. *J. Macromol. Sci., Part A: Pure Appl.Chem.* **2016**, *53*, 276−281.
(39) Zhu, J.; Wei, S.; Gu, H.; Rapole, S. B.; Wang, Q.; Luo, Z.; Haldolaarachchige, N.; Young, D. P.; Guo, Z. Synthesis of magnetic graphene nanocomposites decorated with core@double-shell nanoparticles for fast chromium removal. *Environ. Sci. Technol.* **2012**, *46*, 977−985.
(40) Lingamdinne, L. P.; Koduru, J. R.; Karri, R. R. A comprehensive review of applications of magnetic graphene oxide based nanocomposites for sustainable water purification. *J. Environ. Manage.* **2019**, *231*, 622−634.
(41) Yuan, X.; Chai, Y.; Yuan, R.; Zhao, Q. Improved potentiometric response of solid-contact lanthanum (III) selective electrode. *Anal. Chim. Acta* **2013**, *779*, 35−40.
(42) Zhu, J.; Wei, S.; Haldolaarachchige, N.; Young, DP.; Guo, Z. Electromagnetic Field Shielding Polyurethane Nanocomposites Reinforced with Core−Shell Fe−Silica Nanoparticles. *J. Phys. Chem. C* **2019**, *115*, 15304−15310.
(43) Liu, X.; Zhang, H.; Ma, Y.; Wu, X.; Meng, L.; Guo, Y.; Yu, G.; Liu, Y. Graphene-coated silica as a highly efficient sorbent for residual organophosphorus pesticides in water. *J. Mater. Chem. A* **2013**, *1*, 1875−1884.
(44) Zhao, J.; Wang, Z.; Zhao, Q.; Xing, B. Adsorption of phenanthrene on multilayer graphene as affected by surfactant and exfoliation. *Environ. Sci. Technol.* **2014**, *48*, 331−339.
(45) Kumeria, T.; Bariana, M.; Altalhi, T.; Kurkuri, M.; Gibson, C. T.; Yang, W.; Losic, D. Graphene oxide decorated diatom silica particles as new nano-hybrids, towards smart natural drug microcarriers. *J. Mater. Chem. B* **2013**, *1*, 6320.
(46) Stöber, W.; Fink, A.; Bohn, E. Controlled growth of monodisperse silica spheres in the micron size range. *J. Colloid Interface Sci.* **1968**, *26*, 62−69.
(47) Saner, B.; Dinç, F.; Yürüm, Y. Utilization of multiple graphene nano sheets in fuel cells: The effect of oxidation process on the characteristics of graphene nanosheets. *Fuel* **2011**, *90*, 2609−2616.
(48) Kassaee, M. Z.; Motamedi, E.; Majdi, M. Magnetic Fe3O4-graphene oxide/polystyrene, Fabrication and characterization of a promising nanocomposite. *Chem. Eng. J.* **2011**, *172*, 540−549.
(49) Kou, L.; Gao, C. Making silica nanoparticle-covered graphene oxide nanohybrids as general building blocks for large-area superhydrophilic coatings. *Nanoscale* **2011**, *3*, 519−528.
(50) Wang, T. T.; Lan, J.; Zhang, Y.; Wu, Z. L.; Li, C. M.; Wang, J.; Huang, C. Z. Reduced graphene oxide gated mesoporous silica nanoparticles as a versatile chemo-photothermal therapy system through pH controllable release. *J. Mater. Chem. B* **2015**, *3*, 6377−6384.
(51) Lotya, M.; Rakovich, A.; Donegan, J. F.; Coleman, J. N. Measuring the lateral size of liquid-exfoliated nanosheets with dynamic light scattering. *Nanotechnology* **2013**, *24*, 265703.
(52) Amaro-Gahete, J.; Benítez, A.; Otero, R.; Esquivel, D.; Jiménez-Sanchidrián, C.; Morales, J.; Caballero, Á.; Romero-Salguero, F. J. A comparative study of particle size distribution of graphene nanosheets synthesized by an ultrasound-assisted method. *Nanomaterials* **2019**, *9*, 152.
(53) Vazquez, N. I.; Gonzalez, Z.; Ferrari, B.; Castro, Y. Synthesis of mesoporous silica nanoparticles by sol-gel as nanocontainer for future drug delivery applications. *Bol. Soc. Esp. Ceram.* **2017**, *56*, 139−145.
(54) Olle, E. W.; Ren, X.; McClintock, S. D.; Warner, R. L.; Deogracias, M. P.; Johnson, K. J.; Colletti, L. M. Matrix metalloproteinase-9 is an important factor in hepatic regeneration after partial hepatectomy in mice. *Hepatology* **2006**, *44*, 540.
(55) Campbell, E.; Hasan, M. T.; Pho, C.; Callaghan, K.; Akkaraju, G. R.; Naumov, A. V. Graphene Oxide as a Multifunctional Platform for Intracellular Delivery, Imaging, and Cancer Sensing. *Sci. Rep.* **2019**, *9*, 416.
(56) Ahmad, T.; Rhee, I.; Hong, S.; Chang, Y.; Lee, J. Ni-Fe2O4 nanoparticles as contrast agents for magnetic resonance imaging. *J. Nanosci. Nanotechnol.* **2011**, *11*, 5645.
(57) Seabra, A. B.; Paula, A. J.; de Lima, R.; Alves, O. L.; Durán, N. Nanotoxicity of Graphene and Graphene Oxide. *Chem. Res. Toxicol.* **2014**, *27*, 159−168.
(58) Wang, Y.; Li, Z.; Wang, J.; Li, J.; Lin, Y. Graphene and graphene oxide, biofunctionalization and applications in biotechnology. *Trends Biotechnol.* **2011**, *29*, 205−212.
(59) Shadjou, N.; Hasanzadeh, M.; Khalilzadeh, B. Graphene based scaffolds on bone tissue engineering. *Bioengineered* **2018**, *9*, 38−47.
(60) Justino, C. I. L.; Gomes, A. R.; Freitas, A. C.; Duarte, A. C.; Rocha-Santos, T. A. P. Graphene based sensors and biosensors. *Trends Anal. Chem.* **2017**, *91*, 53−66.
(61) Mansilla Wettstein, C.; Bonafé, F. P.; Oviedo, M. B.; Sánchez, C. G. Optical properties of graphene nanoflakes, Shape matters. *J. Chem. Phys.* **2016**, *144*, 224305.
(62) Hu, W.; Li, Z.; Yang, J. Electronic and optical properties of graphene and graphitic ZnO nanocomposite structures. *J. Chem. Phys.* **2013**, *138*, 124706.
(63) Crowder, S. W.; Prasai, D.; Rath, R.; Balikov, D. A.; Bae, H.; Bolotin, K. I.; Sung, H.-J. Three-dimensional graphene foams promote osteogenic differentiation of human mesenchymal stem cells. *Nanoscale* **2013**, *5*, 4171−4176.
(64) Kim, T.-H.; Lee, T.; El-Said, W.; Choi, J.-W. Graphene- based materials for stem cell applications. *Materials* **2015**, *8*, 8674−8690.
(65) Ahmed, M. S.; Bin Salam, A.; Yates, C.; Willian, K.; Jaynes, J.; Turner, T.; Abdalla, M. Double-receptor-targeting multifunctional iron oxide nanoparticles drug delivery system for the treatment and imaging of prostate cancer. *Int. J. Nanomed.* **2017**, *12*, 6973−6984.
(66) Shen, Z.; Wu, A.; Chen, X. Iron Oxide Nanoparticle Based Contrast Agents for Magnetic Resonance Imaging. *Mol. Pharm.* **2017**, *14*, 1352−1364.

https://doi.org/10.1021/acsomega.0c05395
ACS Omega 2021, 6, 21194−21206

(67) Hummers, W. S.; Offeman, R. E. Preparation of graphitic oxide. *J. Am. Chem. Soc.* **1958**, *80*, 1339.
(68) Foroutan, T.; Nafar, M.; Motamedi, E. Intraperitoneal injection of graphene oxidenanoparticle accelerates stem cell therapy effects on acute kidney injury. *Stem Cells Cloning: Adv. Appl.* **2020**, *13*, 21−32.

https://doi.org/10.1021/acsomega.0c05395
ACS Omega 2021, 6, 21194−21206